Graphical Table of Contents

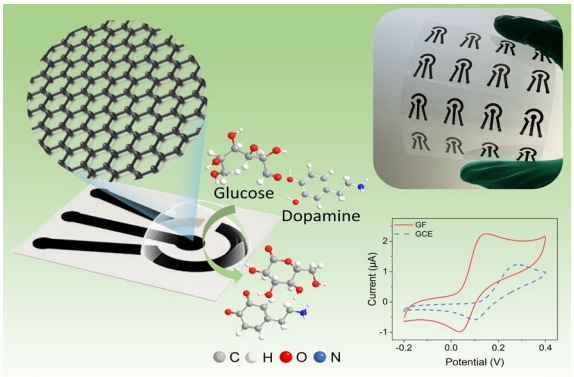

High conductivity graphene films serve as a multifunctional electrode for detection of multiple analytes.

Nano Research, Volume 16, Issue 5, May 2023, pp. 6361-6368
DOI: 10.1007/s12274-023-5459-7

Scalable fabrication of graphene-assembled multifunctional electrode with efficient electrochemical detection of dopamine and glucose

Xiaodong Ji [1], Xin Zhao [2,*], Zixin Zhang [1], Yunfa Si [1], Wei Qian [2], Huaqiang Fu [1], Zibo Chen [1], Zhe Wang [3], Huihui Jin [4,**], Zhugen Yang [5] and Daping He [1,2,***]

[1] State Key Laboratory of Silicate Materials for Architectures, Wuhan University of Technology, Wuhan, 430070, China

[2] Hubei Engineering Research Center of RF-Microwave Technology and Application, Wuhan University of Technology, Wuhan, 430070, China

[3] State Key Laboratory of Advanced Technology for Materials Synthesis and Processing, Wuhan University of Technology, Wuhan, 430070, China

[4] School of Information Engineering, Wuhan University of Technology, Wuhan 430070, China

[5] School of Water, Energy and Environment, Cranfield University, Cranfield, MK43 0AL, UK

[*]Corresponding author.

[**]Corresponding author.

[***]Corresponding author.

Email-address: xzhao@whut.edu.cn (Xin Zhao), jinhuihui@whut.edu.cn (Huihui Jin), hedaping@whut.edu.cn (Daping He)

Abstract

Conventional glassy carbon electrodes (GCE) cannot meet the requirements of future electrodes for wider use due to low conductivity, high cost, non-portability and lack of flexibility. Therefore, cost-effective and wearable electrode enabling rapid and versatile molecule detection is becoming important, especially with the ever-increasing demand for health monitoring and point-of-care diagnosis. Graphene is considered as an ideal electrode due to its excellent physicochemical properties. Here, we prepare graphene-assembled film with ultra-high conductivity and customize the 3-electrode system via a facile and highly controllable laser engraving approach. Benefiting from the ultra-high conductivity (5.65×10^5 S m^{-1}), the 3-electrode system can be used as multifunctional electrode for direct detection of dopamine (DA) and enzyme-based detection of glucose without further metal deposition. The dynamic ranges from 1-200 μM and 0.5-8.0 mM were observed for DA and glucose, respectively with a limit of detection (LOD) of 0.6 μM and 0.41 mM. Overall, the excellent target detection capability caused by the ultra-high conductivity and ease modification of graphene films, together with their superb mechanical properties and ease of mass-produced, provides clear potential not only for replacing GCE for various electrochemical studies but also for the development of portable and high-performance electrochemical wearable medical devices.

Keywords: graphene film, ultra-high conductivity, multifunctional electrode, point-of-care diagnosis, wearable medical devices

1 Introduction

The physicochemical properties of electrodes are closely related to the final performance of various electrochemical reactions [1,2], including typical electrocatalytic reactions such as oxygen reduction reaction [3], CO_2 reduction [4], hydrogen evolution reaction [5], as well as the detection of biomolecules such as dopamine (DA) and glucose. Currently, electrochemical reaction is mainly based on modified glassy carbon electrodes (GCE) for further investigation [6,7]. However, only when GCE are modified with highly conductive materials such as conductive graphdiyne, carbon nanotubes or graphene, the electrode can obtain satisfactory performance [8,9]. Moreover, GCE cannot meet the low-cost and flexibility requirements of the more extensive electrode applications in the future.

Due to the limitations of GCE, efforts have been devoted to the fabrication of paper electrochemical electrode for their potential use in field testing [10,11]. Early work on paper-based device by Dungchai and coworkers achieved the quantitative detection of glucose and lactate with carbon-based working electrode fabricated via screen printing technology, which is the most commonly used method to fabricate carbon electrodes on various substrates [12]. Unfortunately, the conductivity of these screen-printed carbon electrodes is still poor, and further deposition of precious metal nanoparticles is often required to improve the quality and accessibility of these electrodes, which drives up the cost and complicates the fabrication process [10,13–15]. Therefore, the facile preparation of highly conductive paper-based electrodes is the key to promote the rapid development of paper-based devices.

Theoretically, the preparation of highly conductive paper-based electrodes certainly requires highly conductive materials, and graphene is considered as an ideal electrode in electrochemical environments due to its excellent electronic properties, chemical stability, and mechanical properties [16–19]. So far, chemical vapor deposition (CVD) is an excellent way to obtain high-quality, large-scale graphene films [20]. However, the CVD method is considerably costly with high risk of sample breakage and contamination during transfer process. Moreover, the graphene film prepared by CVD has low macroscopic strength, thus limiting its application [21]. Currently, graphene electrodes can be prepared on a large scale by conventional processing techniques such as inkjet printing, screen printing and roll coating, but the graphene electrodes prepared by these methods usually have poor electrical conductivity and the properties of graphene films are limited by the presence of adhesives and/or additives [22,23]. Accordingly, the preparation of highly conductive graphene electrodes still remains a huge challenge.

To address this challenge, here we prepare graphene films with ultra-high electrical conductivity on a large scale by high temperature reduction of graphene oxide films with subsequent rolling compression. The graphene film-based electrode was then realized utilizing a one-step laser-engraving method achieving highly controllable and reproducible fabrication of the electrodes. The prepared graphene films (GFs) possess a conductivity of 5.65×10^5 S m^{-1}, rendering excellent electrochemical performance of the device without the need for further metal deposition [24]. Direct detection of dopamine (DA) has been demonstrated using the bare GF-based electrode

with a far better sensitivity than GCE, a limit of detection (LOD) down to 0.6 μM and excellent selectivity. The detection of glucose in real blood samples using an enzyme-based method has also been demonstrated using the same GF-based electrode showing the customizability and versatility of the system. Further, unlike the most conventionally used methods for paper electrochemical devices (e.g. inkjet printing [25], electron-beam evaporation [26]), the strategy described in this paper requires no usage of expensive masks or sophisticated processes, thus enables easy tailoring of the size and shape of the electrodes according to practical requirements which is very favorable for industrial production. Combined with the remarkable mechanical properties of the GFs, the GF-based electrode in this work shows a clear potential for further implementation as portable and wearable devices.

2 Experimental

2.1 Chemicals and reagents

Potassium ferricyanide ($K_3[Fe(CN)_6]$), potassium ferrocyanide ($K_4[Fe(CN)_6]$), potassium chloride (KCl), ascorbic acid (AA), uric acid (UA), glucose, and dopamine (DA) were purchased from Shanghai Macklin Biochemical Co., Ltd., China. Phosphate buffer saline (PBS) and glucose oxidase (GOx) were purchased from Sangon Biotech (Shanghai) Co., Ltd. China. 5wt% Nafion solution, Ag/AgCl gel, graphene oxide (GO), and polyethylene terephthalate (PET) were purchased from Wuxi Chengyi Education Technology Co., Ltd., China.

2.2 Fabrication of GF

The graphene films (GFs) were made from graphene oxide (GO) by thermal

reduction. Specifically, graphene oxide (GO) was dispersed in deionized water to obtain GO suspension with a mass fraction of 4%. The GO suspension was mechanically stirred to obtain GO gel, and then the GO gel was coated to form a GO film. Thereafter, the GO film was first slowly heated to 1300 ℃ and held for 2 h to form a disordered carbon film under argon atmosphere. Then, the carbonized structure was annealed at 2850 ℃ for 1 h to form a fully C-C sp^2 hybridized graphitic structure under argon atmosphere. Finally, the sample was subjected to rolling compression under 200 MPa to obtain the densely packed GF.

2.3 Characterization

The morphology and microstructure of samples were taken on a filed-emission scanning electron microscopy (SEM, JSM-7610F Plus) at an accelerating voltage of 5.0-15.0 kV and high-resolution transmission electron microscopy (HRTEM, JEM-2100F). The crystal information measurements were collected with X-ray diffraction (XRD, Rigaku Smartlab) using Cu Kα (λ=1.5406 Å) radiation. All electrochemical performances were evaluated by an Autolab PGSTAT302N electrochemical workstation (Eco Chemie).

3 Results and discussion

3.1 Design and electrochemical characterization of GF-based 3-electrode system

The preparation process of GF is shown in Fig. 1(a). Firstly, GO film was obtained by scrape coating, and then the high temperature treatment was carried out at different temperatures. Finally, the film was subjected to rolling compression onto PET to obtain the densely packed GF. Such an easy and controlled preparation method for GF predicts

easy scale-up production, which has already been achieved as shown in Fig. S1. The prepared GF film exhibits a relatively flat surface from a macroscopic view taken by a super-large depth of field 3D microscopic system (KEYENCE, VHX-600E) (Fig. 1b). Subsequently, the film was specifically analyzed at the microscopic level by SEM. Fig. 1(c) presents the cross-sectional SEM image of the film, showing that the GF is formed of ordered and densely stacked graphene layers with a thickness of about 56 μm. The wrinkled surface with many micro folds revealed by the top-view SEM image in Fig. 1(d) is conducive to a large surface area. Then, the graphene nanosheets were observed by TEM. As depicted in Fig. 1(e), the wrinkled structure of the nanosheets provides evidence for the flexibility of the films, which is further corroborated by the high tensile strength of GF in Fig. S2 and the digital photograph of the GF folded into a boat and curled onto a glass rod without cracking in Fig. 1(f). Besides, the perfect lattice fringes of the nanosheets shown in Fig. 1(e) further prove that the basic structure of GF is composed of graphene.

In XRD pattern (Fig. 1(g)), the sharp diffraction peak (002) located around 26.5º also provides evidence of the regular packing of graphene layers with an interspacing of ~0.336 nm. In the Raman spectrum shown in the inset of Fig. 1(g), the faint D-band along with the intense G-band indicate excellent lattice integrity of the GF with high degree of graphitization. This is consistent with the strong 2D band at 2714 cm^{-1}. All the above results indicate that the prepared GF have a low-defect and high-density ordered graphene structure, which is conducive to improved electrical conductivity and contributes to the electrochemical and mechanical properties of the material [27].

In this work, the desired electrochemical device was fabricated directly from the GF pressed on polyethylene terephthalate (PET) substrate to ensure overall flexibility. The desired pattern was obtained by engraving the GF with a laser engraving machine (Fig. S3 in the ESM) followed by peeling off the unwanted area as depicted in Fig. 2(a). The patterned device consists of 3 electrodes, namely the graphene working electrode (WE) with a diameter of 3 mm, the graphene counter electrode (CE), and the Ag/AgCl reference electrode (RE) achieved by drop-casting Ag/AgCl gel directly onto the GF. It is worth mentioning that with the proposed fabrication strategy, the device can be batch-manufactured with great preciseness and reproducibility as shown by the digital photograph of the as-prepared electrode array in Fig. 2(b). And these electrodes also provide a means to realize the vision of wearable detection devices attributing to their outstanding mechanical properties (Fig. 2(c)).

To evaluate the electrochemical performance of the as-prepared GF-based 3-electrode system, cyclic voltammetry (CV) measurements were carried out using the solution of 5 mM $K_3[Fe(CN)_6]/K_4[Fe(CN)_6]$ and 0.1 M KCl at various scan rates ranging from 0.05 V s^{-1} to 0.5 V s^{-1} (Fig. 3(a)). Good linearity was observed between both the anodic and cathodic peak currents (I_{pa} and I_{pc}) and the square root of scan rate ($v^{1/2}$) as depicted in Fig. 3(b), which indicates that the redox reaction of the electroactive $[Fe(CN)_6]^{3-/4-}$ on GF-based working electrode involves freely diffusing species as described by the Randles-Sevcik equation [28]. The linear regression equations are $I_{pa}\ (\mu A) = -5.77 + 440.91\ v^{1/2}(V\ s^{-1})$ $(R^2=0.999)$ and $I_{pc}\ (\mu A) = 4.88 - 416.47\ v^{1/2}(V\ s^{-1})$ $(R^2=0.999)$, respectively. According to the Nicholson method [29,30],

the electron transfer rate was calculated to be 3.10×10^{-3} cm s^{-1}, suggesting an efficient electron transfer on the GF-based 3-electrode system. The performance of the Ag/AgCl reference electrode was also evaluated by performing the CV scans at a scan rate of 0.1 V s^{-1} for 10 cycles. As depicted in Fig. 3(c), both the anodic (E_{pa}) and cathodic (E_{pc}) peak potentials remained unchanged after 10 CV scans, indicating the Ag/AgCl reference electrode can provide satisfactory stable reference potentials. Next, We investigate the reproducibility of the devices by monitoring the consistency of the electrochemical behavior of samples fabricated from 10 different batches. As can be seen from Fig. S4 in the ESM, samples from all 10 batches showed similar cathodic DPV peak current in 5 mM $K_3[Fe(CN)_6]/K_4[Fe(CN)_6]$ and 0.1 M KCl and the relative standard deviation (RSD) was calculated to be 0.7%. These results demonstrate the good reproducibility of the GF-based electrode which is readily applicable for large-scale manufacture.

The stability of the devices during the test is also crucial as they need to provide stable results for quantitative measurements. We evaluated the stability of the devices in 5 mM $K_3[Fe(CN)_6]/K_4[Fe(CN)_6]$ and 0.1 M KCl by monitoring the change of cathodic DPV peak current every 5 days. As can be seen from Fig. 3(d), the cathodic DPV peak current has changed by 3.04% after a month, and Fig. S5 in the ESM shows that the surface structure of the GF-based electrode remains the same after the stability test. These results demonstrate the good stability of the GF-based electrode, which strongly support that the GF can be used as a new excellent electrode for electrochemical testing.

3.2 Electrochemical detection of DA

We then tested the possibility of the GF-based electrode for the quantitative measurement of dopamine (DA). DA belongs to the catecholamine family of neurotransmitters, which can regulate various physiological functions of the central nervous system [31,32]. Indeed, alterations in dopamine concentration may cause a variety of diseases and neurological illnesses, such as Parkinson's disease [33], Schizophrenia [34], tics-coprolalia syndrome [35], attention deficit, hyperactivity disorder [36], and so on. Diagnosis of these diseases necessitates accurate measurements of DA concentration in biological samples.

We first characterized the electron transfer of DA on GF-based electrode. DA is itself electroactive and thus requires no further modification of the working electrode. The CV measurements were carried out by directly pipetting 100 μL of 50 μM DA and 0.01 M PBS as shown in Fig. 4(a). Similar linearity was observed between the peak currents and the square root of the scan rates indicating that the redox reactions of DA on the GF-based working electrode is also diffusion limited (Fig. 4(b)). The deviation from linearity and the non-Nernstian response at slow scan rates are due to the quasi-reversibility and possible irreversible chemical reaction involved [37]. The peak-to-peak separation (ΔE_p) of ~91 mV at scan rate of 0.05 V s^{-1} along with the shifting ΔE_p with scan rate further demonstrate the quasi-reversible electrochemical nature of the process. Further, the performance of GF-based electrode and GCE in 50 μM DA and 0.01 M PBS was evaluated as in Fig. 4(c) which demonstrates a higher current response towards DA on GF-based electrodes than on GCE. Electrochemical

impedance spectroscopy (EIS) results show that the R_{ct} of the GF-based electrode (39 Ω) is smaller than that of the GCE (93 Ω) (inset of Fig. 4(c)), indicating that the GF-based electrode allows faster electron transfer, which is consistent with the CV results. Moreover, the GF-based electrode exhibits high conductivity of 5.65×10^5 S m^{-1}, which is 75 times higher than that of GCE (7.55×10^3 S m^{-1}) (Fig. 4d), which also verifies the high current response of the GF-based electrode. On the other hand, the contact angle test shows that the GF has slightly better wettability than GCE (Fig. S6, S7 in the ESM), which facilitates the contact between GF and electrolyte, and also contributes to the higher current response of GF.

We next explore the sensitivity and LOD of the GF-based system for specific detection of DA applying differential pulse voltammetry (DPV). The DPV scans were conducted between -0.2-0.4 V with the optimal conditions as follows: step potential of 5 mV, modulation amplitude of 25 mV, modulation time of 0.05 s, and interval time of 0.5 s. Increased electrochemical responses were observed with increasing concentration of DA as shown in Fig. 5(a). With linear fitting, the dynamic range was determined to be from 1 μM to 200 μM (Fig. 5(b)). The regression equation obtained between the peak currents and concentration of DA was $I_{pa}\ (\mu A)=0.14 + 0.01\ C_{DA}\ (\mu M)$ $(R^2=0.996)$ with a measurable limit of detection (LOD) determined from the standard deviation and slope of the calibration curve with a confidence factor of 3 to be 0.6 μM. The performances of several other carbon-based electrodes for DA sensing reported previously are listed in Table S1 in the ESM for comparison. From the table, the GF-based electrode proposed in this article exhibits a satisfactory linear range and a

relatively low limit of detection.

To fulfill its function as portable and wearable devices, the GF-based electrode needs to deliver unaffected electrochemical signals under various deformations when mounted over curvilinear body parts. The sensing performance of our detection platform under such conditions was validated by deforming the GF-based electrode and then taking the DPV measurements in 50 μM DA. As can be seen from Fig. 5(c), the bending and twisting deformations barely affect the electrochemical performance of the electrode as evidenced by the almost unchanged DPV peak currents compared to its flat state. Simultaneously, the resistance of GF has not changed during 100 times of bending (Fig. S8), showing its excellent flexibility and stability. This superb flexibility and stability favors the potential use of the GF-based electrode in wearable devices.

The capability of selective detection towards DA relative to other bioactive species was also investigated. The elimination of the interference effect of ascorbic acid (AA) has long been a challenging task in the detection of DA since its oxidation peak locates at approximately the same potential as DA. DPV measurements were conducted with 80 μM DA in the presence of equal concentrations of AA. This concentration was chosen based on the highest possible concentration of AA in real samples to the best of our knowledge [38].

As can be seen from Fig. 5(d), the intensity of the oxidation peak is barely affected by the addition of AA compared to the case with DA showing a negligible change of 1.69%. This behavior can be ascribed to the highly sp^2-conjugated structure of the GF that enables the π-π interaction with the phenyl structure in DA [39]. This interaction

effectively promotes the electron transfer between the GF WE and DA and in the meantime restrain the electron transfer between the GF WE and AA. Several other interferences that are commonly present in bio-samples were also considered. The oxidation currents of 80 μM DA showed only negligible changes of 0.87% and 2.42% in the presence of 80 μM UA and 80 μM glucose respectively. Even with the coexistence of all three interfering substances, the oxidation peak intensity of DA only changed by 1.9%., indicating the superb selectivity towards the detection of DA.

3.3 Electrochemical detection of glucose

To demonstrate the capability of the GF-based electrode for not only direct detection of electroactive biological molecules, but also bioreceptor-based sensing (e.g. enzymes, aptamers, antibodies), the working electrode was modified with glucose oxidase (GOx) to assess the performance of specific detection of glucose. To prepare the GOx-modified GF WE, 10 μl of GOx aqueous solution with concentration of 10 $mg \cdot mL^{-1}$ was drop-coated onto the surface of a clean GF WE and let dry at 4 ℃. Then, 5 μl of 0.5%wt Nafion solution was pipetted onto the enzyme-modified electrode to form a uniform protective layer.

CV measurements were carried out using the GOx-modified electrode in N_2-saturated 0.01 M PBS (pH=7.4) at different scan rates. As shown in Fig. 6(a), clearly discernible and well-defined redox peaks were observed with a relatively small peak-to-peak separation of ~87 mV at scan rate of 0.1 $V \cdot s^{-1}$, confirming the efficient electron transfer between the redox center of GOx ($FAD/FADH_2$) and the GF electrode. The relationship between the scan rates and peak currents was also investigated. Within

the range of 0.05 V s^{-1} to 0.3 V s^{-1}, both the cathodic peak and anodic peak currents exhibited linear relationship with the scan rates (Fig. 6(b)) indicative of an adsorption-controlled process due to the redox reaction of the active center of GOx as below.

$$GOx\ (FAD) + 2e^- + 2H^+ \rightarrow GOx\ (FADH_2) \quad (1)$$

Moreover, the electroactive enzyme on the electrode surface can be calculated by the following equation

$$Ip = n^2F^2vA\Gamma/4RT \quad (2)$$

Where n is the electron transfer number, A is the surface area of electrode, v is the scan rate, Γ is the average surface concentration of enzyme, and F, R, and T represent Faraday constant, ideal gas constant, and absolute temperature, respectively. The calculated surface average concentration of GOx immobilized on GF electrode was 5.5×10^{-11} mol cm^{-2}.

The electrocatalytic activity of the Nafion/GOx/GF electrode towards glucose oxidation was studied by recording CV curves in oxygen-saturated PBS solution with different concentrations of glucose. As depicted in Fig. 6(c), with increasing glucose concentration, the reduction current gradually decreased due to the consumption of O_2. The calibration curve shown in Fig. 6(d) indicates a linear relationship between the glucose concentration and reduction current at -0.48 V within a dynamic range from 0.5 to 8.0 mM and the LOD was calculated to be 0.41 mM. The relative standard deviation (RSD) of the reduction peak current with 2.0 mM glucose was calculated to be 6.4% based on 10 successive measurements, demonstrating satisfying stability. The blood

glucose level is normally between 4.0 to 6.0 mM which is within the linear dynamic response range obtained with our Nafion/GOx/GF electrode system.

The performance of the Nafion/GOx/GF electrode towards real sample was evaluated by detecting glucose levels in human blood samples. The samples were collected from 4 healthy volunteers and were then investigated by CV measurements at scan rate of 0.1 V s^{-1}. To mimic the practical real-time application, no pretreatment (e.g. dilution and centrifugation) was performed on these samples. The reduction currents at -0.48 V were substituted into the linear regression equation of the calibration curve to determine the glucose level in the blood samples and the results are summarized in Table S2 in the ESM together with the results measured using commercial glucometer for comparison. It can be seen that the results determined by our device and the commercial electrode are in good agreement yielding a deviation between 0-5.4%.

4 Conclusions

In summary, we have demonstrated a low cost, flexible and sensitive electrode using laser-engraved graphene film (GF) which shows a promise for multiple-target detection for point-of-care testing. The excellent electrical properties of the GF render the device highly efficient electron transfer at the interface of the electrode and the electroactive dopamine (DA), inducing a specific electrochemical response directly related to the concentration of DA. Without the need for any further modification, our bare GF-based electrode is able to detect DA of concentrations as low as 0.6 μM and a linear dynamic response ranging from 1-200 μM. Moreover, the fabricated GF-based 3-electrode system exhibited versatile usage not only for direct detection of

electroactive biomolecules but also for enzyme-based detection. Successful detection of glucose using glucose oxidase (GOx) has been achieved with dynamic range from 0.5 to 8.0 mM, indicating the feasibility of surface modification of the GF-based electrode for a broad spectrum of applications such as biomedical diagnosis, environmental monitoring, and food safety. Due to the excellent property of graphene film, the GF-based electrode shows significant potential as a new platform for the implementation of wearable devices for continuous health and disease monitoring.

Acknowledgements

This work was supported by the National Natural Science Foundation of China (51672204, 22102128), the Fundamental Research Funds for the Central Universities (WUT: 2021IVA66; WUT:2022IVA172; WUT: 2020IB005).

References

[1] Yang, J. R.; Li, W. H.; Xu, K. N.; Tan, S. D.; Wang, D. S.; Li, Y. D. Regulating the tip effect on single-atom and cluster catalysts: forming reversible oxygen species with high efficiency in chlorine evolution reaction. *Angew. Chem. Int. Ed.* **2022**, *61*, e202200366.

[2] Li, W. H.; Yang, J. R.; Wang, D. S. Long-range interactions in diatomic catalysts boosting electrocatalysis. *Angew. Chem. Int. Ed.* **2022**, e202213318.

[3] Chen, R.; Shu, T.; Zhao, F. L.; Li, Y. F.; Yang, X. T.; Li, J. W.; Zhang, D. L.; Gan, L. Y.; Yao, K. X.; Yuan, Q. $PtCu_3$ nanoalloy@porous PWOx composites with oxygen container function as efficient ORR electrocatalysts advance the power density of room-temperature hydrogen-air fuel cells. *Nano Res.* **2022**, *15*,

9010–9018.

[4] Zhang, Z. D.; Zhu, J. X.; Chen, S. H; Sun, W. M. Wang, D. S. Liquid fluxional Ga single atom catalysts for efficient electrochemical CO_2 reduction. *Angew. Chem. Int. Ed.* **2022**, e202215136.

[5] Liu, Z. H.; Du, Y.; Yu, R. H.; Zheng, M. B.; Hu, R.; Wu, J. S.; Xia, Y. Y.; Zhuang, Z. C.; Wang, D. S. Tuning mass transport in electrocatalysis down to sub-5nm through nanoscale grade separation. *Angew. Chem. Int. Ed.* **2022**, e202212653.

[6] Shen, L.; Liang, Z.; Chen, Z. Y.; Wu, C.; Hu, X. F.; Zhang, J. Y; Jiang, Q.; Wang, Y. B. Reusable electrochemical non-enzymatic glucose sensors based on Au-inlaid nanocages. *Nano Res.* **2022**, *15*, 6490-6499.

[7] Long, B. J.; Cao, P. Y.; Zhao, Y. M.; Fu, Q. Q.; Mo, Y.; Zhai, Y. M.; Liu, J. J.; Lyu, X. Y.; Li, T.; Guo, X. F. et al. Pt_1/Ni_6Co_1 layered double hydroxides/n-doped graphene for electrochemical non-enzymatic glucose sensing by synergistic enhancement of single atoms and doping. *Nano Res.* **2022**.

[8] Zhou, Q.; Li, G. H.; Zhang, Y. J.; Zhu, M.; Wan, Y. K.; Shen, Y. F. Highly selective and sensitive electrochemical immunoassay of Cry1C using nanobody and π-π stacked graphene oxide/thionine assembly. *Anal. Chem.* **2016**, *88*, 9830–9836.

[9] Long, B. J.; Zhao, Y. M.; Cao, P. Y.; Wei, W.; Mo, Y.; Liu, J. J.; Sun, C. J.; Guo, X. F.; Shan, C. S.; Zeng, M. H. Single-atom Pt boosting electrochemical nonenzymatic glucose sensing on $Ni(OH)_2$/n-doped graphene. *Anal. Chem.* **2022**, *94*, 1919–1924.

[10] Yu, H. X.; Chen, Z. M.; Liu, Y. Z.; Alkhamis, O.; Song, Z. P.; Xiao, Y. Fabrication of aptamer-modified paper electrochemical devices for on-site biosensing. *Angew. Chem. Int. Ed.* **2021**, *60*, 2993–3000.

[11] Mahato, K.; Wang, J. Electrochemical sensors: from the bench to the skin. *Sensors Actuators, B Chem.* **2021**, *344*, 130178.

[12] Dungchai, W.; Chailapakul, O.; Henry, C. S. Electrochemical detection for paper-based microfluidics. *Anal. Chem.* **2009**, *81*, 5821–5826.

[13] Wang, C.; Wu, R.; Ling, H.; Zhao, Z.; Han, W.; Shi, X.; Payne, G.F.; Wang, X. Toward scalable fabrication of electrochemical paper sensor without surface functionalization. *npj Flex. Electron.* **2022**, *6*, 12.

[14] Metters, J. P.; Kadara, R. O.; Banks, C. E. New directions in screen printed electroanalytical sensors: an overview of recent developments. *Analyst* **2011**, *136*, 1067.

[15] Duan, W. C.; del Campo, F. J.; Gich, M.; Fernández-Sánchez, C. In-field one-step measurement of dissolved chemical oxygen demand with an integrated screen-printed electrochemical sensor. *Sensors Actuators B Chem.* **2022**, *369*, 132304.

[16] Valentine, C. J.; Takagishi, K.; Umezu, S.; Daly, R.; De Volder, M. Paper-based electrochemical sensors using paper as a scaffold to create porous carbon nanotube electrodes. *ACS Appl. Mater. Interfaces* **2020**, *12*, 30680–30685.

[17] Liu, N.; Chortos, A.; Lei, T.; Jin, L. H.; Kim, T. R.; Bae, W. G.; Zhu, C. X.; Wang, S. H.; Pfattner, R.; Chen, X. Y. et al. Ultratransparent and stretchable graphene

electrodes. *Sci. Adv.* **2017**, *3*, e1700159.

[18] Zhu, Y. Q.; Cao, T.; Cao, C. B.; Luo, J.; Chen, W. X.; Zheng, L. R.; Dong, J. C.; Zhang, J.; Han, Y. H.; Li, Z. et al. One-pot pyrolysis to n-doped graphene with high-density Pt single atomic sites as heterogeneous catalyst for alkene hydrosilylation. *ACS Catal.* **2018**, *8*, 10004–10011.

[19] Xu, Q.; Zhang, J.; Wang, D. S.; Li, Y. D. Single-atom site catalysts supported on two-dimensional materials for energy applications. *Chinese Chem. Lett.* **2021**, *32*, 3771–3781.

[20] De Fazio, D.; Purdie, D. G.; Ott, A. K.; Braeuninger-Weimer, P.; Khodkov, T.; Goossens, S.; Taniguchi, T.; Watanabe, K.; Livreri, P.; Koppens, F. H. L. et al. High-mobility, wet-transferred graphene grown by chemical vapor deposition. *ACS Nano* **2019**, *13*, 8926–8935.

[21] Liu, F. N.; Li, P.; An, H.; Peng, P.; McLean, B.; Ding, F. Achievements and challenges of graphene chemical vapor deposition growth. *Adv. Funct. Mater.* **2022**, *32*, 2203191.

[22] Orzari, L. O.; Cristina de Freitas, R.; Aparecida de Araujo Andreotti, I.; Gatti, A.; Janegitz, B. C. A novel disposable self-adhesive inked paper device for electrochemical sensing of dopamine and serotonin neurotransmitters and biosensing of glucose. *Biosens. Bioelectron.* **2019**, *138*, 111310.

[23] He, W. Z.; Liu, R. T.; Zhou, P.; Liu, Q. Y.; Cui, T. H. Flexible micro-sensors with self-assembled graphene on a polyolefin substrate for dopamine detection. *Biosens. Bioelectron.* **2020**, *167*, 112473.

[24] Zhao, X.; He, D.; You, B. Laser engraving and punching of graphene films as flexible all-solid-state planar micro-supercapacitor electrodes. *Mater. Today Sustain.* **2022**, *17*, 100096.

[25] Lemarchand, J.; Bridonneau, N.; Battaglini, N.; Carn, F.; Mattana, G.; Piro, B.; Zrig, S.; Noël, V. Challenges, prospects, and emerging applications of inkjet-printed electronics: a chemist's point of view. *Angew. Chem. Int. Ed.* **2022**, *61*, e202200166.

[26] Chakraborty, B.; Saha, R.; Chattopadhyay, S.; De, D.; Das, R.D.; Mukhopadhyay, M.K.; Palit, M.; RoyChaudhuri, C. Impact of surface defects in electron beam evaporated ZnO thin films on FET biosensing characteristics towards reliable PSA detection. *Appl. Surf. Sci.* **2021**, *537*, 147895.

[27] Li, P.; Yang, M. C.; Liu, Y. J.; Qin, H. S.; Liu, J. R.; Xu, Z.; Liu, Y. L.; Meng, F. X.; Lin, J. H.; Wang, F. et al. Continuous crystalline graphene papers with gigapascal strength by intercalation modulated plasticization. *Nat. Commun.* **2020**, *11*, 2645.

[28] Khaliliazar, S.; Öberg Månsson, I.; Piper, A.; Ouyang, L.; Réu, P.; Hamedi, M. M. Woven electroanalytical biosensor for nucleic acid amplification tests. *Adv. Healthc. Mater.* **2021**, *10*, 2100034.

[29] Randviir, E. P. A cross examination of electron transfer rate constants for carbon screen-printed electrodes using electrochemical impedance spectroscopy and cyclic voltammetry. *Electrochim. Acta* **2018**, *286*, 179–186.

[30] Nicholson, R. S. Theory and application of cyclic voltammetry for measurement of electrode reaction kinetics. *Anal. Chem.* **1965**, *37*, 1351–1355.

[31] Heien, M. L. A. V; Khan, A. S.; Ariansen, J. L.; Cheer, J. F.; Phillips, P. E. M.; Wassum, K. M.; Wightman, R. M.; Murray, R. W. Real-time measurement of dopamine fluctuations after cocaine in the brain of behaving rats. *Proc. Natl. Acad. Sci. U. S. A.* **2005**, *102*, 10023-10028.

[32] Liu, M. L.; Chen, Q.; Lai, C. L.; Zhang, Y. Y.; Deng, J. H.; Li, H. T.; Yao, S. Z. A double signal amplification platform for ultrasensitive and simultaneous detection of ascorbic acid, dopamine, uric acid and acetaminophen based on a nanocomposite of ferrocene thiolate stabilized Fe_3O_4@Au nanoparticles with graphene sheet. *Biosens. Bioelectron.* **2013**, *48*, 75–81.

[33] Zhuang, X.; Mazzoni, P.; Kang, U. J. The role of neuroplasticity in dopaminergic therapy for parkinson disease. *Nat. Rev. Neurol.* **2013**, *9*, 248–256.

[34] Grace, A. A. Dysregulation of the dopamine system in the pathophysiology of schizophrenia and depression. *Nat. Rev. Neurosci.* **2016**, *17*, 524–532.

[35] Pan, Z. L.; Guo, H.; Sun, L.; Liu, B. Q.; Chen, Y.; Zhang, T. T.; Wang, M. Y.; Peng, L. P.; Yang, W. A novel electrochemical platform based on COF/La_2O_3/MWCNTs for simultaneous detection of dopamine and uric acid. *Colloids Surf. A Physicochem. Eng. Asp.* **2021**, *635* 128083.

[36] Klein, M. O.; Battagello, D. S.; Cardoso, A. R.; Hauser, D. N.; Bittencourt, J. C.; Correa, R. G. Dopamine: functions, signaling, and association with neurological diseases. *Cell. Mol. Neurobiol.* **2019**, *39*, 31–59.

[37] Elgrishi, N.; Rountree, K. J.; McCarthy, B. D.; Rountree, E. S.; Eisenhart, T. T.; Dempsey, J. L. A practical beginner's guide to cyclic voltammetry. *J. Chem. Educ.*

2018, *95*, 197–206.

[38] Khamcharoen, W.; Siangproh, W. A multilayer microfluidic paper coupled with an electrochemical platform developed for sample separation and detection of dopamine. *New J. Chem.* **2021**, *45*, 12886–12894.

[39] Wang, Y.; Li, Y. M.; Tang, L. H.; Lu, J.; Li, J. H. Application of graphene-modified electrode for selective detection of dopamine. *Electrochem. commun.* **2009**, *11*, 889–892.

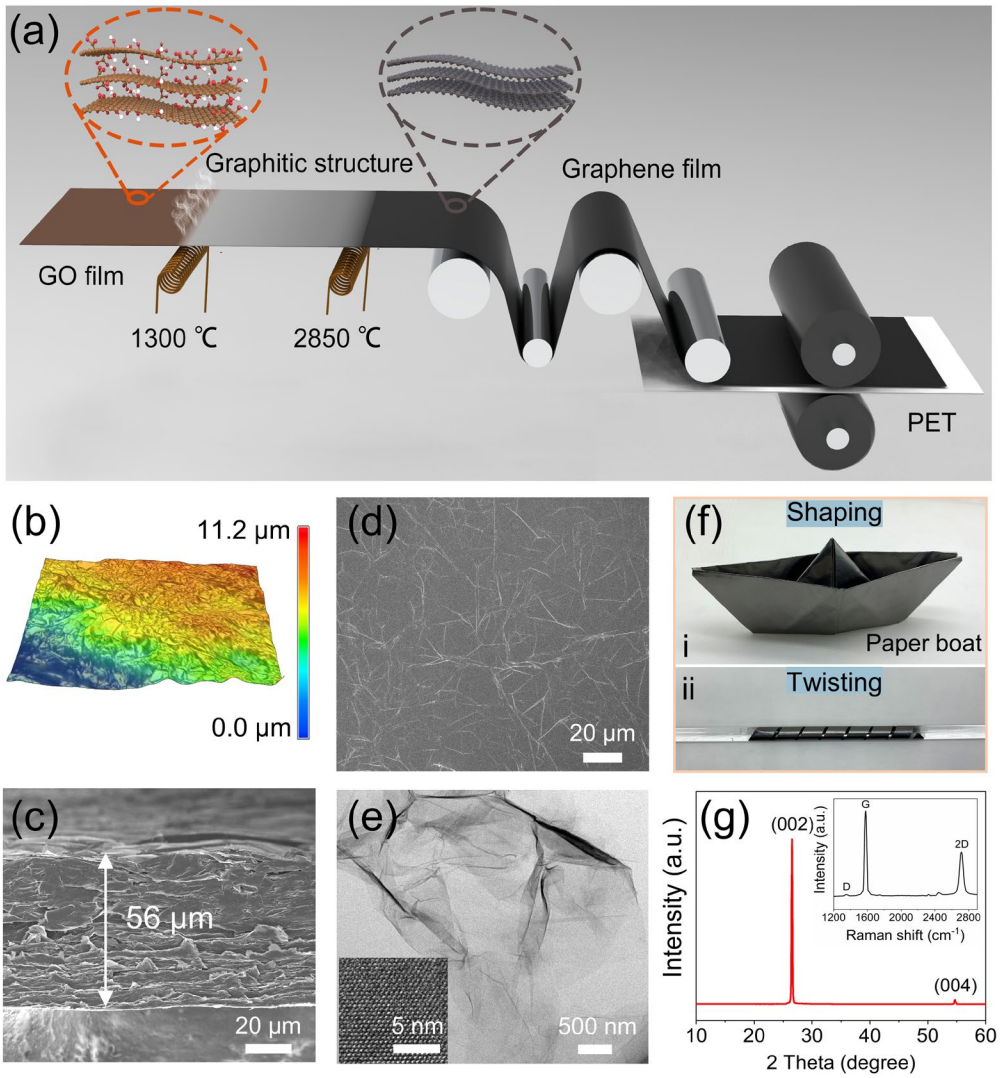

Figure 1 Fabrication and characterization of the graphene-assembled film (GF). (a) Fabrication process of GF involving high-temperature annealing and rolling compression. (b) The surface picture of the GF taken by a super-large depth of field 3D microscopic system. (c) Cross-sectional SEM image of the GF. (d) Surface SEM image of the GF. (e) TEM image of the graphene nanosheets from the GF (inset: HRTEM image of the graphene nanosheets from the GF). (f) Digital photographs of the prepared GF folded into a boat (i) and curled along a glass rod (ii) demonstrating superb flexibility. (g) XRD pattern of GF (inset: Raman spectrum of GF).

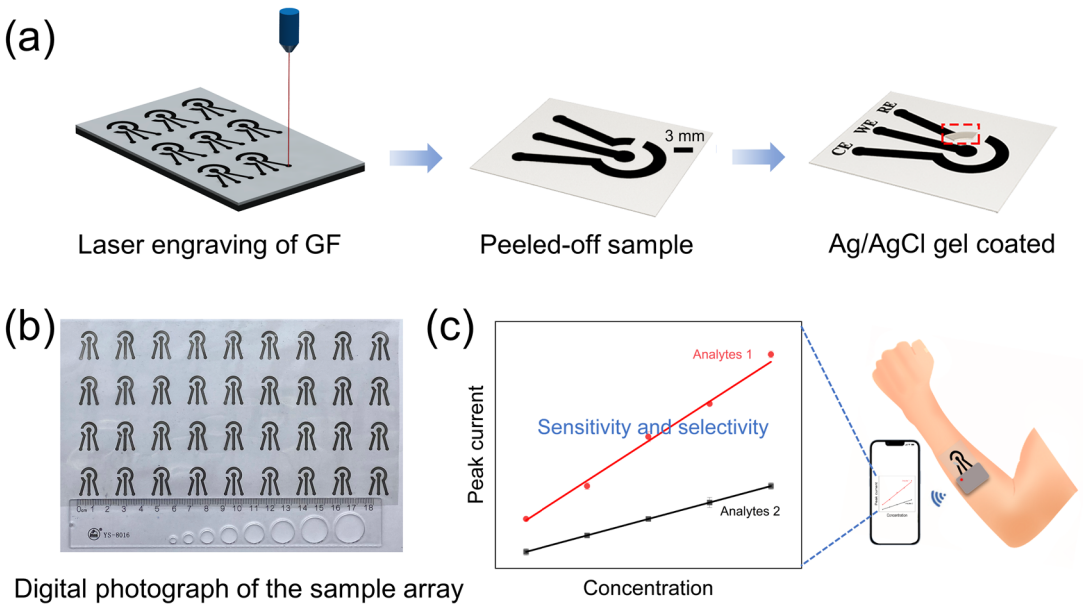

Figure 2 Fabrication and measurement setup of the GF-based 3-electrode system. (a) Schematic illustration showing the laser engraving process on GF to fabricate the GF-based 3-electrode system. (b) Digital photograph showing the as-prepared electrode array on PET substrate. (c) Schematic diagram of the wearable electrode for portable electrochemical detection.

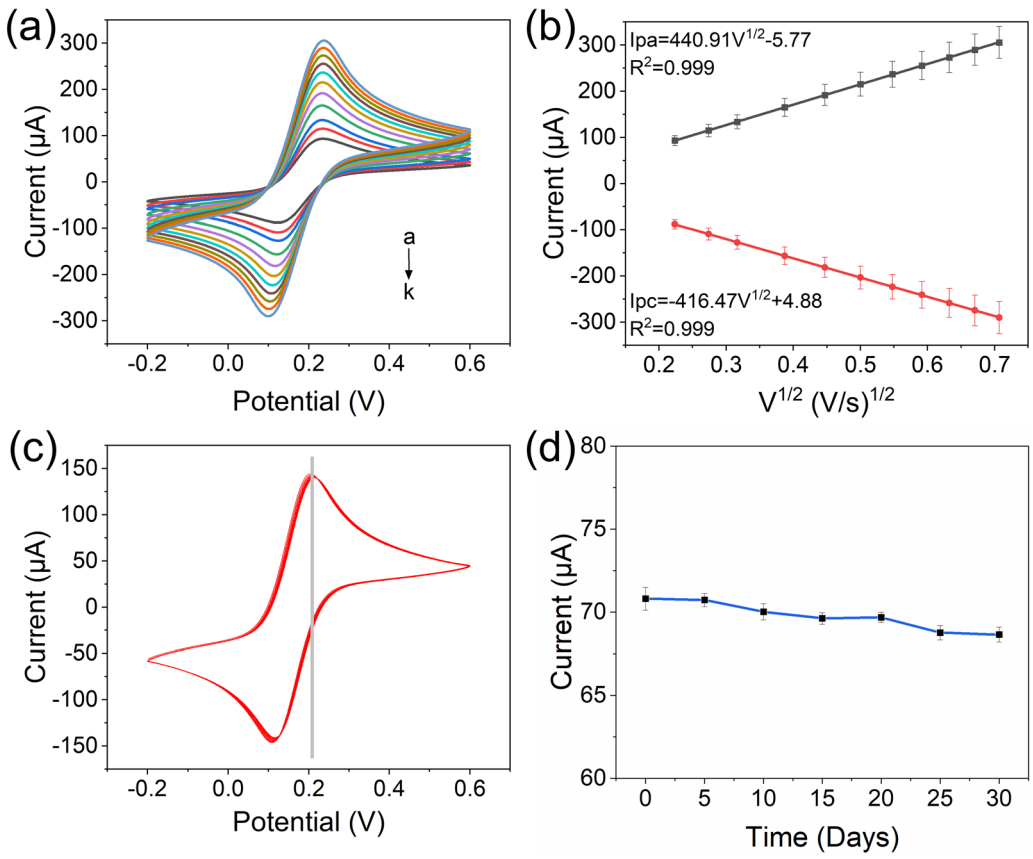

Figure 3 Electrochemical performance of GF-based electrode in 5 mM $K_3[Fe(CN)_6]/K_4[Fe(CN)_6]$ and 0.1 M KCl. (a) Cyclic voltammetry measurements conducted at different scan rates (a-k: 0.05, 0.75, 0.1, 0.15, 0.2, 0.25, 0.3, 0.35, 0.4, 0.45 and 0.5 V s^{-1}). (b) The peak current plotted as a function of the square root of the scan rate with the fitted linear regression curves. Black and red dots indicate anodic and cathodic peak currents, respectively. (c) 10 cycles of CV recorded at scan rate of 0.1 V s^{-1}. (d) Stability test of the GF-based electrode with different times. Error bars were obtained from 3 successive DPV measurements with the same device.

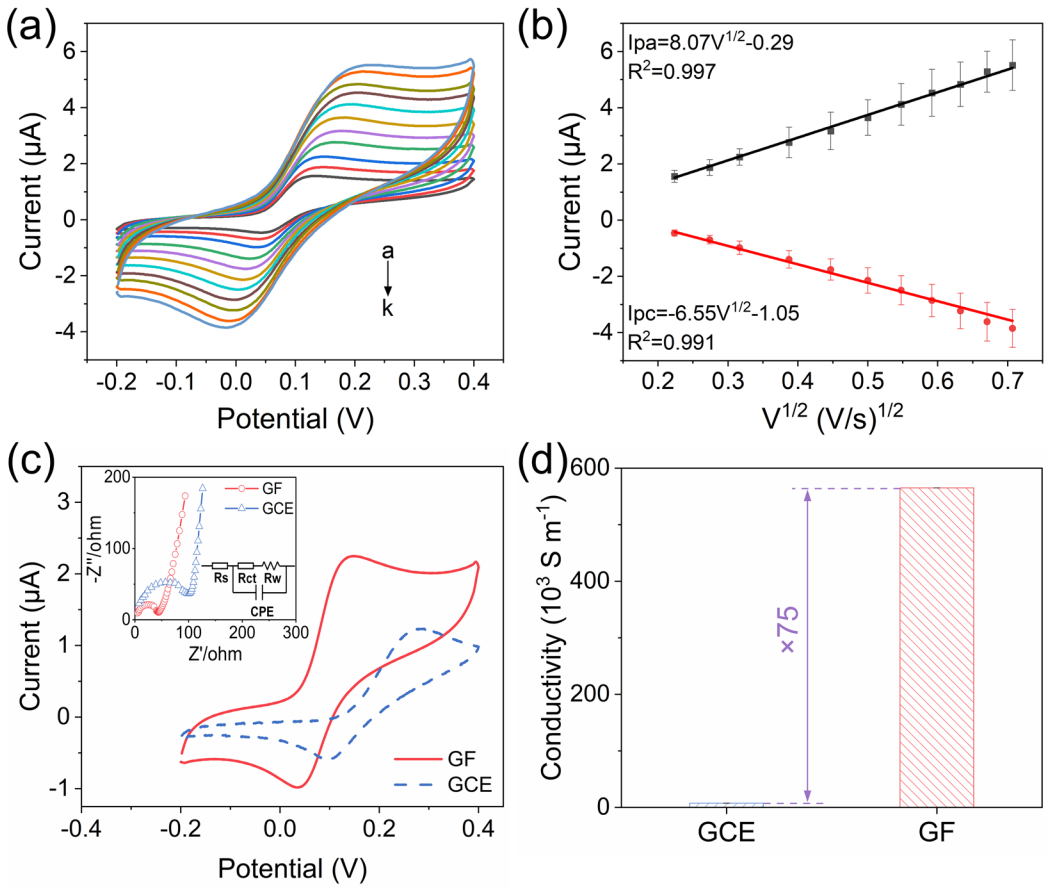

Figure 4 Electrochemical performance of GF-based electrode in 50 μM DA and 0.01 M PBS. (a) Cyclic voltammetry measurements conducted at different scan rates (a-k: 0.05, 0.75, 0.1, 0.15, 0.2, 0.25, 0.3, 0.35, 0.4, 0.45 and 0.5 V s^{-1}). (b) The peak current plotted as a function of the square root of the scan rate with the fitted linear regression curves. Black and red dots indicate anodic and cathodic peak currents, respectively. (c) CV curves of GF-based electrode and glassy carbon electrode (inset: Nyquist plots of GF-based electrode and glassy carbon electrode with equivalent circuit). (d) Comparison of conductivities of GF-based electrode and glassy carbon electrode.

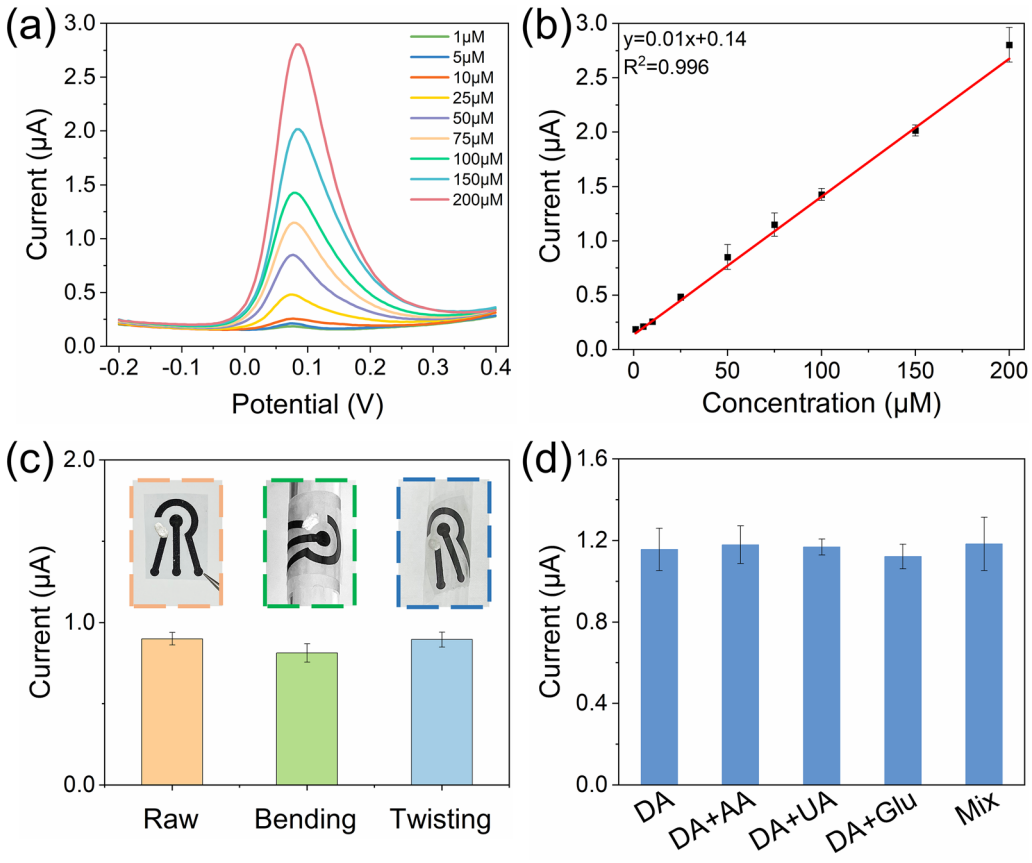

Figure 5 DA detection using the GF-based electrode. (a) DPV curves measured with different concentrations of DA using the GF-based electrode. (b) The fitted calibration curve of the GF-based electrode between the peak currents and DA concentrations. (c) Effects of bending and twisting deformations of the GF-based electrode on the electrochemical response towards DA. (d) Evaluation of selectivity for DA using the GF-based electrode.

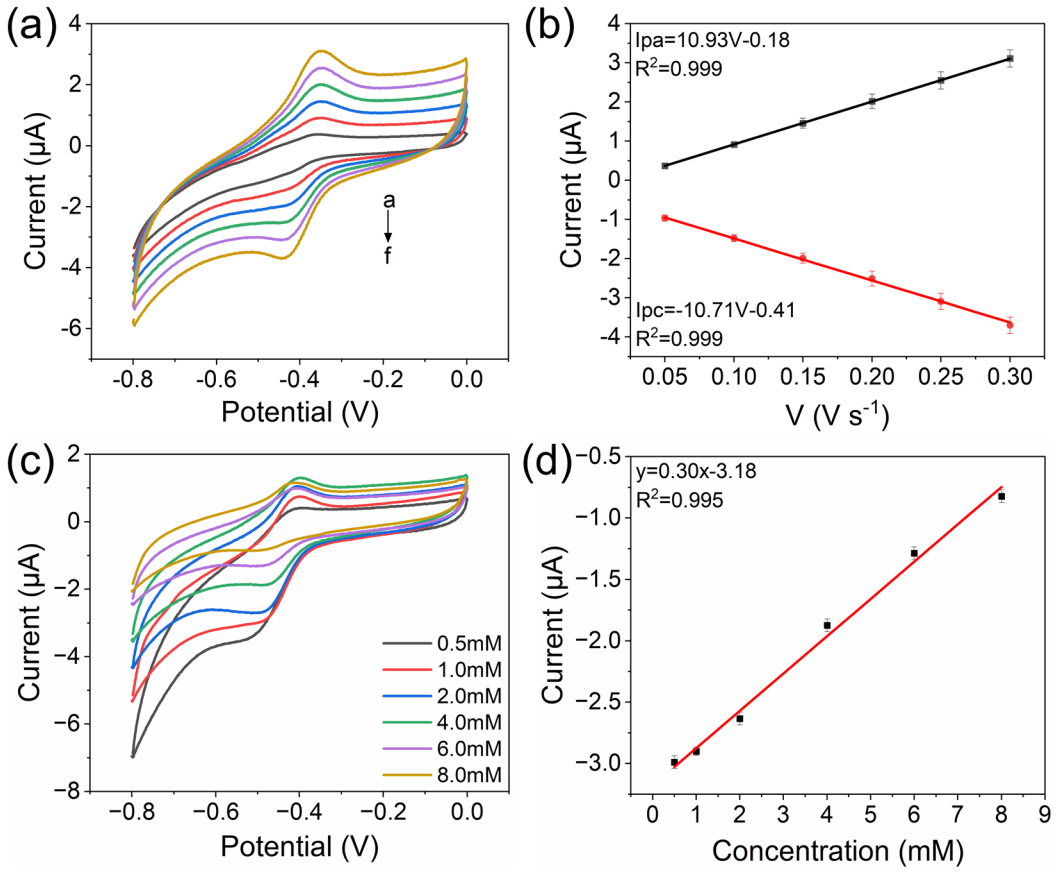

Figure 6 Glucose detection using the Nafion/GOx/GF electrode. (a) Cyclic voltammograms of the Nafion/GOx/GF electrode in 0.01 M N_2-saturated PBS solution (pH 7.4) at different scan rates of 0.05, 0.10, 0.15, 0.20, 0.25, and 0.30 $V \cdot s^{-1}$. (b) The peak current plotted as a function of the scan rate with the fitted linear regression curves. Black and red dots indicate anodic and cathodic peak currents, respectively. (c) CV curves of Nafion/GOx/GF electrode in O_2-saturated PBS buffer (pH 7.4) with different glucose concentrations. (scan rate = 0.1 V s^{-1}). (d) The fitted calibration curve of the Nafion/GOx/GF electrode between the cathodic peak intensities and concentrations of glucose.